Effects of Sr2+-substitution on the reduction rates of Yz* in PSII membranes--evidence for concerted hydrogen-atom transfer in oxygen evolution.

ARTICLE *in* BIOCHEMISTRY · DECEMBER 2000

Impact Factor: 3.02 · Source: PubMed

4 AUTHORS, INCLUDING:

Nikos Lydakis Simantiris
Technological Educational Institute of Crete
44 PUBLICATIONS **864** CITATIONS

Effects of Sr^{2+}-Substitution on the Reduction Rates of $Y_z^{\bullet}$ in PSII Membranes—Evidence for Concerted Hydrogen-Atom Transfer in Oxygen Evolution†

Kristi L. Westphal,‡ Nikos Lydakis-Simantiris,§ Robert I. Cukier, and Gerald T. Babcock*

Department of Chemistry, Michigan State University, East Lansing, Michigan 48824

Received August 1, 2000; Revised Manuscript Received October 20, 2000

ABSTRACT: Several groups have recently investigated the kinetic effects of biochemical treatments, site-directed mutagenesis, or substitution of essential cofactors on the stepwise, water-oxidizing chemistry catalyzed by Photosystem II. Consistently, these studies show evidence for a slowing of the final, oxygen-releasing step, $S_3 \rightarrow S_0$, of the catalytic cycle. To a degree, some of this work also shows a slowing of the earlier S-state transitions. To study these processes in more detail, we have investigated the effect of replacing Ca^{2+} with Sr^{2+}on the rates of the S-state transitions by using time-resolved electron paramagnetic resonance. The results show a slowdown of the last transition in the cycle, consistent with a report from Boussac et al. [Boussac, A., Sétif, P., and Rutherford, A. W. (1992) *Biochemistry 31*, 1224−1234], and of the earlier S-state transitions as well, which suggests that a common molecular mechanism is at work and that Sr^{2+} is less effective than Ca^{2+} in supporting it. While the oxidation of Y_z by P_{680}^+ has been extensively studied and can be understood within the context of nonadiabatic electron tunneling combined with rapid, non-rate-limiting proton transfer in the holo-system [Tommos, C., and Babcock, G. T. (2000) *Biochim. Biophys. Acta 1458*, 199], the reduction of $Y_z^{\bullet}$ by the Mn cluster cannot be described effectively by a nonadiabatic electron-transfer formalism. This indicates that this reaction is rate limited by processes other than electron tunneling. We discuss our results for $Y_z^{\bullet}$ reduction and those of others for the activation parameters (E_a, A, KIE, and rates) associated with this process, in terms of both sequential and concerted proton-coupled, electron transfer. Our analysis indicates that concerted hydrogen-atom transfer processes best explain the observed characteristics of the S-state advances.

Oxygen evolution in photosynthesis results from light-driven water oxidation that is catalyzed by Photosystem II (PSII).[1] The catalytic site is composed of a tetrameric manganese cluster and a redox-active tyrosine, Y_z, that has been identified as tyrosine 161 of the D1 protein (for reviews see refs *1*−*3*). A histidine at the D1 190 position is the initial acceptor of the phenol proton released upon Y_Z oxidation by the reaction center chlorophyll complex, P_{680} (*4*−*9*). In close proximity to the catalytic center are two ions, Ca^{2+} and Cl^-, that are needed for efficient oxygen evolution (*10*−*12*), but their exact roles are still under investigation. Bound to PSII on the inside of the thylakoid membrane are three extrinsic polypeptides with molecular masses of 17, 23, and 33 kDa. They have been implicated in the prevention of Ca^{2+} and Cl^- migration out of the catalytic site and also as stabilizers of the structure of the Mn complex. Although progress has been made recently on obtaining structural information for two- and three-dimensional crystals of PSII, these have not yet been solved to high resolution (*13*).

Catalysis is initiated by the absorption of a photon of light by P_{680}. In its excited state, P_{680} ultimately transfers an electron to a quinone, Q_A, thereby forming the charge-separated state, $P_{680}^+Q_A^-$. The subsequent reduction of P_{680}^+ is carried out by Y_z, which is, in turn, reduced by the substrate water/Mn cluster. This process occurs with the absorption of each photon as the Mn cluster accumulates the four oxidizing equivalents necessary to split water. The intermediates at the substrate water/Mn cluster that result from this photochemistry are designated by the S_n notation, where n is the number of stored oxidizing equivalents (*14*, *15*). After formation of S_4, O_2 is released and the system resets to S_0.

The rates at which these oxidation steps occur were first measured by Babcock et al. by using time-resolved electron paramagnetic resonance (EPR) spectroscopy and were shown to vary with the oxidation state of the Mn cluster (*16*). More recent studies by Razeghifard et al. have shown that these rates can be altered when the OEC is chemically, biochemically, or genetically modified (*17*−*19*). The exact mechanism

† This work was supported by USDA CRGO (G.T.B.), by NIH GM37300 (G.T.B.), and by NIH GM47274 (R.I.C.).

* To whom correspondence should be addressed.

‡ Current address: Department 9N6, Building AP20, Abbott Laboratories, 100 Abbott Park Road, Abbott Park, IL 60064.

§ Current Address: Mediterranean Agronomic Institute of Chania, Crete, Greece.

[1] Abbreviations: A, preexponential factor; E_a, activation energy; EGTA, ethylene glycol bis(β-aminoethyl ether)-*N*,*N*,*N*′,*N*′-tetraacetic acid; EPR, electron paramagnetic resonance; ET/PT, electron transfer followed by proton transfer; ETPT, concerted electron and proton transfer; KIE, kinetic isotope effect; MES, morpholinoethanesulfonic acid; $(Mn)_4$, tetramanganese cluster; MSP, manganese stabilizing protein; OEC, oxygen-evolving complex; PPBQ, phenyl-*p*-benzoquinone; P_{680}, photoactive chlorophyll of PSII; PSII, Photosystem II; PT/ET, proton transfer followed by electron transfer; Q_A, primary plastoquinone acceptor; S_n, redox state of the oxygen evolving complex; TS, transition state; Y_z, tyrosine 161 of the D1 polypeptide.

10.1021/bi0018077 CCC: $19.00
Published on Web 11/30/2000

by which this occurs is unknown, but it has been proposed that the effect is general and not specific to an S-state transition or to the type of modification performed (*20*, *21*).

To probe the effects of these treatments on the rates of the catalytic cycle, PSII membranes were depleted of Ca^{2+} and subsequently reconstituted with Sr^{2+}. Reconstitution of the sample by the addition of Sr^{2+} allows for about 40% of oxygen-evolving activity to be recovered (*22*, *23*). Previous time-resolved EPR studies have shown that in these reconstituted samples the oxygen releasing step, $S_3 \rightarrow S_0$, is slowed about 20 times compared to the native system (*24*). In addition, a 5-fold decrease in rates of the $S_3 \rightarrow S_0$ transition was shown with samples that were reconstituted with Ca^{2+} instead of Sr^{2+} (*24*). These results clearly show both local protein and cofactor impact for the final S-state transition that releases O_2. However, to identify the effects of these sample modifications as general, the rates of the other S-state transitions require investigation. The aim of this work is to study more closely the rates of $Y_z^{\bullet}$ reduction by the substrate water/Mn cluster during earlier S-state transitions, to interpret these results within the context of current models for water splitting and to consider the underlying mechanism for $Y_z^{\bullet}$ reduction.

MATERIALS AND METHODS

PSII membranes were prepared from fresh market spinach according to the method of Berthold et al. (*25*) with the modifications described in ref *26*. They were stored in 0.4 M sucrose, 15 mM NaCl, and 50 mM MES/NaOH, pH 6.0, at −80 °C until use. Salt-washed membranes were prepared as in Boussac and Rutherford (*23*). The PSII particles were washed in room light for 30 min at 4 °C at 0.5 mg of chlorophyll/mL in a SMN buffer containing 0.3 M sucrose, 1.2 M NaCl, and 25 mM MES, pH 6.5, and then centrifuged. The pellet was resuspended in a SMN buffer made up of 0.3 M ultrapure sucrose (Aristar, BDH Laboratory Supplies, United Kingdom), 30 mM NaCl, 50 μM EGTA, and 25 mM MES, pH 6.5, and then centrifuged. The pellet was resuspended and centrifuged a second time before the final product was resuspended in a SMN buffer containing 0.3 M sucrose, 15 mM NaCl, and 25 mM MES, pH 6.5, to a final concentration of 2 mg/mL. For the pH studies, the salt-washed BBYs were resuspended in the same buffer, but at a pH of 5.9, 6.5, or 7.1. Prior to flash-illumination, PPBQ and ferricyanide were added to final concentrations of 100 μM and 1 mM, respectively. $SrCl_2$ or $CaCl_2$ was added to salt-washed samples to a final concentration of 15 mM.

EPR spectroscopy was performed at room temperature with a Bruker ESP 300E spectrometer equipped with a TM_{011} cavity. The spectrometer was tuned to the low-field peak of the stable $Y_D^{\bullet}$ radical (D2-Y160) and kinetic traces for Y_Z oxidation and subsequent reduction were recorded at this field value. The experiments under steady-state flashing light conditions were carried out by using a 350 μL capacity suprasil quartz flat cell (Wilmad, Buena, NJ). Each sample received 100 flashes before being replaced by a fresh sample. For the S-state-resolved studies, a home-built, continuous-flow system was used to provide fresh samples to the flat cell mounted in the cavity. Each sample received a train of three flashes before being replaced. A pump (Gilson, Inc., Middleton, WI) was used to control the flow rate so that a fresh, dark-adapted sample was supplied for each flash sequence. Following flash illumination, the sample was recycled to a reservoir that was held at 4 °C and kept in absolute darkness for 15 min. Each experiment was completed in approximately 5 h with about 2000 scans averaged. Photoexcitation of the sample was accomplished by using a Quanta-Ray DCR-11 pulsed Nd:YAG laser (Spectra-Physics, Mountain View, CA). A personal computer equipped with a Metrabyte WAAG board and a Metrabyte CTM-05 timing board was used to trigger both the EPR spectrometer and the laser (*27*). The EPR conditions for each experiment are given in the figure legends. A least-squares fitting routine (Origin 5.0, Microcal Software, Inc., Northampton, MA) was used to analyze the kinetic traces.

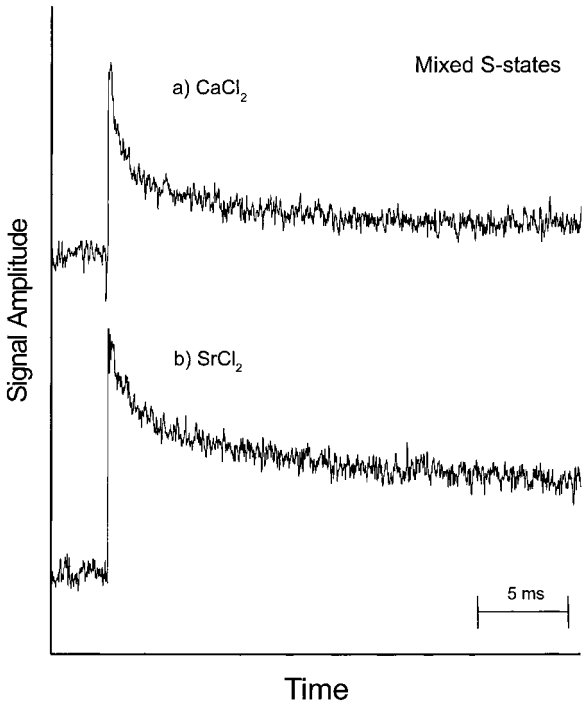

FIGURE 1: Time-resolved EPR steady-state kinetic traces for $Y_z^{\bullet}$ reduction in salt-washed PSII membranes reconstituted with (a) $CaCl_2$ or (b) $SrCl_2$. Experimental conditions: Time constant 40 μs, modulation amplitude 4 G, gain 1×10^5, microwave power 3 dB, frequency 9.78 GHz, magnetic field locked at low-field $Y_z^{\bullet}$ peak (3470 G), room temperature, flash frequency 0.66 Hz. A total of 2000 events was averaged.

Oxygen evolution activity was measured with a Clark-type electrode under continuous illumination with saturating white light from two projector lamps of 250 W each. Oxygen evolution rates for intact BBYs were typically between 650 and 750 μmol O_2/mg Chl h while salt-washed, Ca^{2+} and Sr^{2+} reconstituted samples were typically 450−550 and 200−300 μmol of O_2/mg of Chl h, respectively. Ferricyanide and DCBQ, at concentrations of 600 and 300 μM, respectively, were used as the electron acceptors for these measurements.

RESULTS

S-State Mixed Kinetics. Figure 1 shows the kinetic EPR traces of the decay of $Y_z^{\bullet}$ in salt-washed PSII membranes reconstituted with either Ca^{2+} (trace a) or Sr^{2+} (trace b) under steady-state flashing light conditions. The number of spins was determined by comparing the amplitudes of each kinetic trace to one obtained under the same experimental conditions

for a tris-washed sample, which generates 1 $Y_z^\bullet$ spin/reaction center (*28*). Using this procedure, we estimate that 0.5 spins/reaction center for the Ca^{2+}-reconstituted sample was produced on each flash, which is in agreement with values reported by this laboratory (*27*) and reports on intact PSII membranes by other labs (*18*, *29*). The Sr^{2+}-reconstituted sample, however, showed a 20% increase in spins due to slow $Y_z^\bullet$ reduction in the $S_0 \rightarrow S_1$ transition, which is sufficiently retarded in the Sr^{2+} sample that its detection is now possible (see below). The lower apparent $Y_z^\bullet$ spin count in O_2-evolving samples relative to tris-washed material may be due to broadening of its EPR signal by the $(Mn)_4$ cluster. In Ca^{2+}-depleted samples, $Y_z^\bullet$ is in close association with Mn, which broadens its EPR signal at lower temperatures (*30*−*32*). Similar effects could operate in O_2-evolving samples and cause an apparent decrease in spin concentration.

Each kinetic trace in Figure 1 shows a biphasic decay. For the Ca^{2+}-reconstituted sample, the fast phase, which is approximately 50% of the total amplitude, is attributed to the reactions $S_1Y_z^\bullet \rightarrow S_2Y_z$ and $S_2Y_z^\bullet \rightarrow S_3Y_z$, while the slow phase, which is approximately 35% of the total amplitude, is produced from the $S_3Y_z^\bullet \rightarrow [S_4] \rightarrow S_0Y_z$ reaction. The remaining 15% of the total amplitude is attributed to the decay of $Y_z^\bullet$ in damaged centers that behave like tris-washed PSII membranes. A laser flash artifact is detected on each flash and does not completely cancel with subtraction of an off-resonance trace obtained at 3400 G. This should not greatly interfere with the rate determination of the decaying phases of the kinetic traces. The Ca^{2+}-reconstituted sample (trace a) shows half-times of ∼300 μs and ∼4 ms for the fast and slow phase, respectively. The Sr^{2+}-reconstituted sample (trace b) has a greater amplitude owing to contributions to the fast phase by $S_0 \rightarrow S_1$. The half-times are ∼900 μs and ∼15 ms for the fast and slow phase, respectively. Comparisons of the two kinetic traces in Figure 1 show that Sr^{2+}-reconstitution slows the rate of $Y_z^\bullet$ reduction on all S-state transitions and also shows an increase in the signal amplitude due to the additional detection of $S_0 \rightarrow S_1$.

S-State Resolved Kinetics. To study the effects of Sr^{2+}-reconstitution on the rates of $Y_z^\bullet$ reduction in more detail, we resolved the S-state transitions individually. A sample that was poised primarily in the S_1 state by pre-flash and subsequent dark adaptation was flowed into the flat cell and given three saturating flashes. The flow rate was adjusted so that each sample received three flashes spaced 100 ms apart before it was replaced by the next dark-adapted aliquot. The first flash initiated the transition $S_1Y_z^\bullet \rightarrow S_2Y_z$, while the second flash generated primarily $S_2Y_z^\bullet \rightarrow S_3Y_z$. The final flash caused $Y_z^\bullet$ reduction on the $S_3Y_z^\bullet \rightarrow [S_4] \rightarrow S_0Y_z$ transition, with a small contribution from the other states that is caused by double hits and misses. Figure 2 shows kinetic traces and best fits for the first flash given to salt-washed PSII membranes reconstituted with either Ca^{2+} (trace a) or Sr^{2+} (trace b). Both traces show biphasic behavior with the fast phase being attributed to the decay of $Y_z^\bullet$ upon the $S_1Y_z^\bullet \rightarrow S_2Y_z$ transition and the slow phase to reduction of $Y_z^\bullet$ in damaged centers. The reduction of $Y_z^\bullet$ on the first flash for the Ca^{2+}-reconstituted sample (trace a) has a half-time of ∼200 μs. The Sr^{2+}-reconsitituted sample displayed slower reduction kinetics on the S_1 $Y_z^\bullet \rightarrow S_2Y_z$ transition (trace b) with a half-time of ∼900 μs. The spin counts for the above kinetic traces were 0.40 and 0.90 for Ca^{2+}-reconstituted and Sr^{2+}-reconstituted samples, respectively. The greater number of spins from the Sr^{2+}-reconstituted sample was in part due to the additional detection of the $S_0 \rightarrow S_1$ transition, to Y_z sites in centers deficient in O_2 evolution, and to $Y_D^\bullet$ generation on the first flash. The remaining increase is most likely due to S-state dependent effects caused by magnetic interaction between the tyrosyl radical and the manganese cluster that produce small differences in the $Y_z^\bullet$ line shape. These later effects will not substantially alter the fast kinetics that are the primary focus of this study and will therefore not be discussed further.

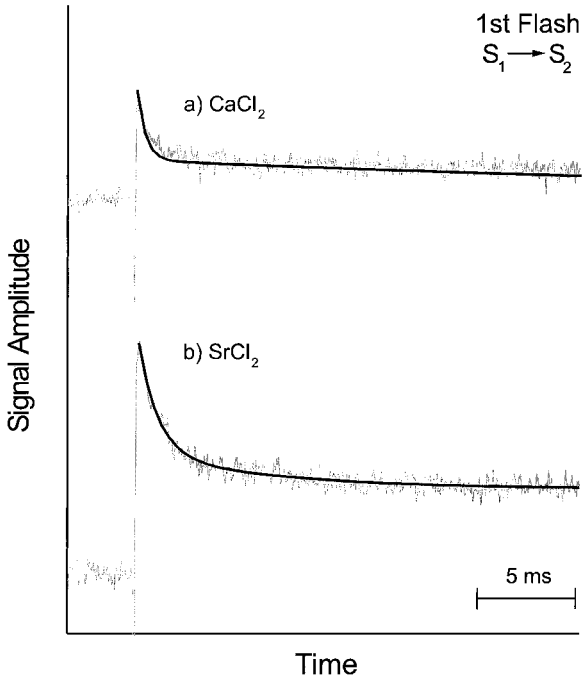

FIGURE 2: Time-resolved EPR kinetic traces for the $S_1Y_z^\bullet \rightarrow S_2Y_z$ transition triggered by the first flash in a three flash experiment. Salt-washed PSII membranes reconstituted with (a) $CaCl_2$ or (b) $SrCl_2$ were used. Experimental conditions: time constant 20 μs in panel a and 40 μs in panel b, modulation amplitude 4 G, gain 1×10^5, microwave power 3 dB, frequency 9.78 GHz, magnetic field locked at low-field peak (3470 G), room temperature. 4000 events were averaged.

The kinetic traces for the second transition are shown in Figure 3. The S-state advance, $S_2Y_z^\bullet \rightarrow S_3Y_z$, showed a slowing in the Sr^{2+}-reconstituted sample that was similar to that of the first flash. The half-times calculated for the Ca^{2+}-reconstituted and Sr^{2+}-reconstituted samples were ∼450 μs and ∼1.3 ms, respectively. The spin count, 0.50, is nearly the same for both sample types. Figure 4 shows the kinetic traces for Ca^{2+}- and Sr^{2+}-reconstituted samples on the $S_3Y_z^\bullet \rightarrow [S_4] \rightarrow S_0Y_z$ transition. Due to mixing of the S-state transitions by the third flash, the decays also had a small contribution from the earlier and faster S-state transitions. In addition, the amplitude of these traces increased, compared to the second flash, to a spin count of about 0.55. The half-times were ∼5.0 and ∼18 ms for Ca^{2+}- and Sr^{2+}-reconstituted samples, respectively.

Effects of pH and Isotope Exchange. The effects of pH on the reduction rates of $Y_z^\bullet$ in the salt-washed, Sr^{2+}-reconstituted samples were investigated to determine if a pH shift occurs for S-state advance upon cation substitution. The effects of pH were studied by carrying out the S-state resolved, three-flash experiment at pH values of 5.9, 6.5,

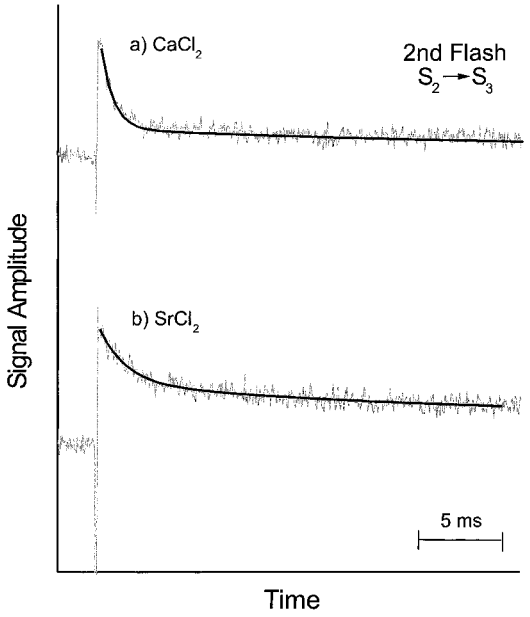

FIGURE 3: Time-resolved EPR kinetic traces for the $S_2Y_z^{\bullet} \rightarrow S_3Y_z$ transition triggered by the second flash in a three flash experiment. Salt-washed PSII membranes reconstituted with (a) $CaCl_2$ or (b) $SrCl_2$ were used. Experimental conditions: time constant 20 μs in panel a and 40 μs in panel b, modulation amplitude 4 G, gain 1×10^5, microwave power 3 dB, frequency 9.78 GHz, magnetic field locked at low-field peak (3470 G), room temperature. A total of 4000 events was averaged.

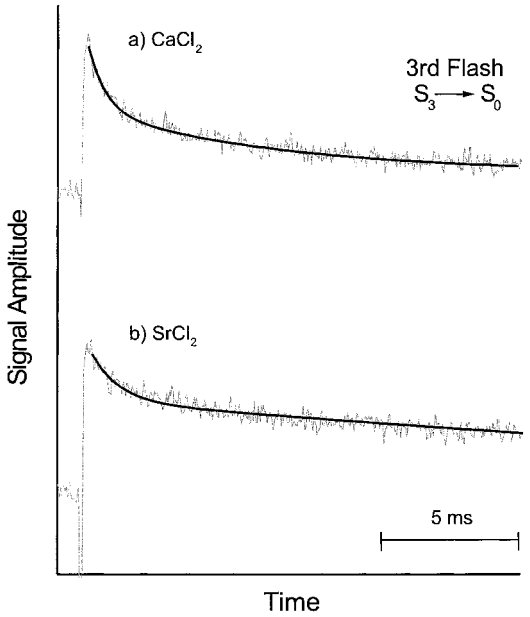

FIGURE 4: Time-resolved EPR kinetic traces for the $S_3Y_z^{\bullet} \rightarrow S_0Y_z$ transition triggered by the third flash in a three flash experiment. Salt-washed PSII membranes reconstituted with (a) $CaCl_2$ or (b) $SrCl_2$ were used. Experimental conditions: time constant 20 μs in panel a and 40 μs in panel b, modulation amplitude 4 G, gain 1×10^5, microwave power 3 dB, frequency 9.78 GHz, magnetic field locked at low-field peak (3470 G), room temperature. A total of 4000 events was averaged.

and 7.1 in Sr^{2+}-reconstituted samples. The results of this experiment, shown in Figure 5, indicate that there is no substantial effect of pH on the kinetics of $Y_z^{\bullet}$ reduction by the Mn cluster in the 5.9−7.1 range. A similar lack of pH effects in the physiological range have been reported earlier for the unperturbed, O_2-evolving system (*33*).

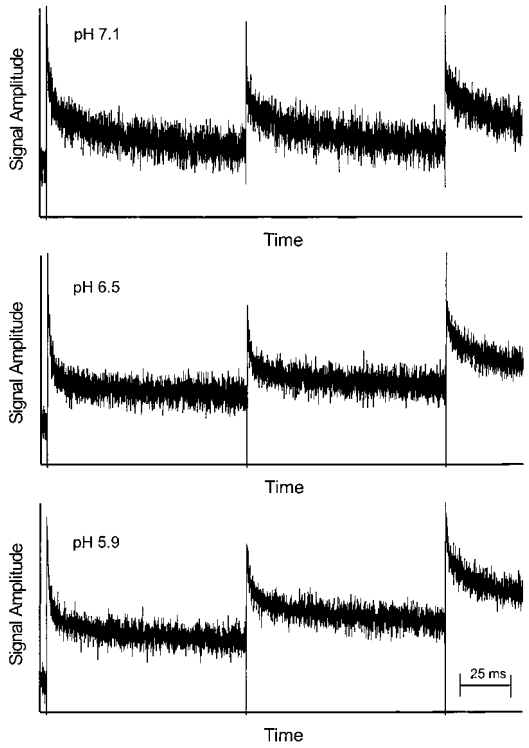

FIGURE 5: Time-resolved EPR kinetic traces for the $S_1Y_z^{\bullet} \rightarrow S_2Y_z$, $S_2Y_z^{\bullet} \rightarrow S_3Y_z$, $S_3Y_z^{\bullet} \rightarrow S_0Y_z$ transitions in salt-washed, Sr^{2+}-reconstituted PSII membranes resuspended in buffers at pH 5.9, 6.5, and 7.1. Experimental conditions: Time constant 40 μs, modulation amplitude 4 G, gain 1×10^5, microwave power 3 dB, frequency 9.78 GHz, magnetic field locked at low-field peak (3470 G), room temperature. A total of 2000 events were averaged.

In addition, an isotope effect study was performed. Salt-washed BBYs were exchanged into a MN buffer containing 15 mM NaCl, 25 mM MES (pD 6.5) in 99.9% D_2O with a final addition of 15 mM $SrCl_2$. The preparation of the sample was identical to that of the experiments performed above on samples in H_2O, except that the buffers used did not contain sucrose since sucrose contains several exchangeable protons and the final washing steps were performed in a D_2O-MN buffer. The rate of isotope exchange has been shown to occur in a matter of minutes or less, well within the time it takes to carry out the final washing steps (*21*, *34*−*36*). Analysis of the flash-induced kinetic traces in a steady-state experiment shows a kinetic isotope effect similar to that reported for the intact system (*37*−*39*) with a maximal value of about 1.4 (Figure 6).

DISCUSSION

The data presented in Table 1 show that Sr^{2+} reconstitution produces a situation whereby the substrate water/Mn cluster is less facile in reducing $Y_z^{\bullet}$, relative to the unmodified system. All S-state transitions show slower kinetics, with the largest effect seen on the last transition. For this step, the rate slows by more than 10-fold, from 1.4 ms in intact PSII membranes to about 18 ms in Sr^{2+} reconstituted membranes, consistent with the observations of Boussac et al. (*24*). A decrease of $S_3 \rightarrow [S_4] \rightarrow S_0$ has been reported for various treatments that affect the water splitting complex. For example, the depletion/repletion of Ca^{2+} (*24*, *40*), the depletion/repletion of Cl^- (*41*), or the removal of the 33 kDa protein (*19*) has been shown to slow the $S_3 \rightarrow [S_4] \rightarrow S_0$ transition. The earlier transitions may have been affected as

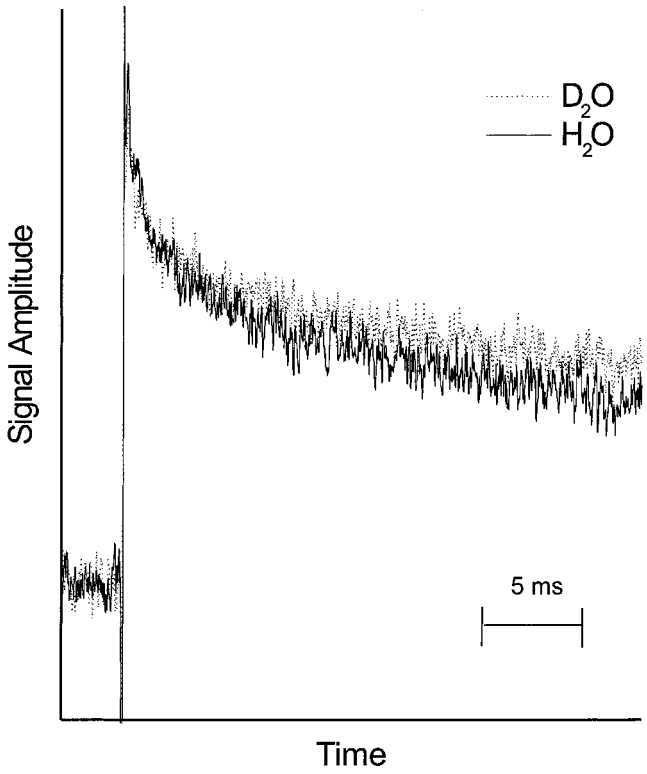

FIGURE 6: Kinetic isotope effect studies using time-resolved EPR. Steady-state kinetic traces for $Y_z^\bullet$ reduction in salt-washed PSII membranes reconstituted with $SrCl_2$ in H_2O or D_2O. Experimental conditions: time constant 40 μs, modulation amplitude 4 G, gain 1×10^5, microwave power 3 dB, frequency 9.78 GHz, magnetic field locked at low-field peak (3470 G), room temperature, flash frequency 0.66 Hz. A total of 2000 events was averaged.

well, but measurements aimed at exploring this possibility were not reported. Studies on Cl^--depleted PSII membranes, performed by van Gorkom and co-workers, demonstrated a slowing of the final step of the S-state cycle upon the reconstitution of the sample with different anionic cofactors (*41*). Razeghifard et al. showed that $Y_z^\bullet$ reduction was slowed to approximately 9 ms on the $S_3 \rightarrow [S_4] \rightarrow S_0$ transition in an engineered strain lacking the Mn-stabilizing protein. Despite these variations in $Y_z^\bullet S_3$ reaction rates, Pace and co-workers have demonstrated for a variety of modified systems that O_2 release and $Y_z^\bullet$ reduction are concomitant (*18*, *19*), consistent with the original interpretation of Babcock et al. that $Y_z^\bullet$ reduction rate limits O_2 evolution (*16*).

While these treatments have been studied only for the $S_3 \rightarrow [S_4] \rightarrow S_0$ transition, other perturbations have been shown to produce a slowing of earlier S-state transitions. For example, the rates of all the S-state transitions are dependent upon the degree to which the system is perturbed in the preparation of PSII membranes. Razeghifard et al. showed that the treatment of thylakoids to prepare PSII membranes leads to retardation of all S-state transitions, with the largest effect seen on the last transition (*17*, *18*). The mutation work done by Hundelt et al. on D1-Asp61 also demonstrated slower $Y_z^\bullet$ reduction rates (*42*). When this aspartate was mutated to the uncharged species, asparagine, oxygen evolution was retained, but the S-state transitions were retarded. The $S_1 \rightarrow S_2$ and $S_2 \rightarrow S_3$ transitions were slowed by a factor of 2−3, while the oxygen-evolving step was slowed by a factor of 9−10.

These various perturbing conditions lead to a common observable: a slow of the reduction of $Y_z^\bullet$ by the substrate water/Mn cluster. Most have been shown to delay the last transition, the oxygen evolving step, and others also show a retardation of the earlier S-state transitions (see Table 1 for a complete summary of half-times). A molecular basis for this kinetic modification is unclear, as is whether this modification is a general effect seen on all S-state transitions or is specific to an S-state or specific to the treatment.

Sr^{2+} replacement for Ca^{2+} provides an excellent probe to address these issues. There is a large decrease in the $S_3 \rightarrow [S_4] \rightarrow S_0$ rate induced by cofactor substitution (*24*) and recent models for oxygen evolution postulate specific, but distinct, roles for Ca^{2+} that fall into one of two categories. In the first, direct involvement of Ca^{2+} in the formation of the oxygen molecule has been suggested (*43*−*45*). For the second, a more general role for Ca^{2+} involves assisting in the catalytic efficiency of the OEC (*20*, *46*).

In the first case, the removal of Ca^{2+} would be expected to deter the formation of the O−O bond on the $S_3 \rightarrow [S_4] \rightarrow [S_4] \rightarrow [S_4] \rightarrow [S_4] \rightarrow S_0$ transition. Pecoraro et al. and Limburg et al. postulated that Ca^{2+} presents a hydroxide nucleophile close enough to a putative $Mn^{V}{=}O$ species to form the critical O−O bond in the S_4 state (*43*, *47*). Siegbahn and Crabtree have also employed Ca^{2+} in O−O bond formation to provide a solution to the energetic difficulty of forming the reactive oxyl radical (*44*). The proposed five-coordinate, Mn−oxo complex generated in S_3 is unreactive and incapable of forming an O−O bond until it chelates with the calcium complex to become six-coordinate. This allows the reactive $Mn^{IV}-O^\bullet$ complex to form, which subsequently leads to O−O bond formation. In these models, O−O bond formation cannot occur without Ca^{2+} in the site, but the cycle of events prior to this step is not expected to be influenced significantly by the depletion of this cofactor. This is especially so if some or all S-state transitions correspond to pure electron tunneling (*48*), as there appears to be consensus that little structural alteration accompanies Ca^{2+} replacement by Sr^{2+} in the OEC (*49*−*51*). Likewise, there is no indication of a dramatic change in driving force for S-state advance when cofactor substitution is carried out. If Sr^{2+} substitution

Table 1: Half-Times for S-State Advance in Various PSII Preparations

						Ca^{2+}-depleted PSII membranes reconstituted with the following ions		Ca^- depleted PSII membranes reconstituted with the following ions				
S-state	thylakoids	PSII membranes	PSII core particles	D61N	l-MSP	Ca^{2+}-	Sr^{2+}-	Cl^-	Br^-	NO_3^-	NO_2^-	I^-
$Y_z^\bullet S_1 \rightarrow Y_z S_2$	65−86 μs	30−70 μs	75−95 μs	240 μs	nd	200 μs	900 μs	nd	nd	nd	nd	nd
$Y_z^\bullet S_2 \rightarrow Y_z S_3$	140−245 μs	55−110 μs	225−380 μs	520 μs	nd	450 μs	1300 μs	nd	nd	nd	nd	nd
$Y_z^\bullet S_3 \rightarrow Y_z S_0$	750 μs; 1.3 ms	1.2−1.4 ms	4.1−4.6 ms	nd	6.0 ms	5.0 ms	18 ms	3.3	4.9	15.6	8.2	11.7
ref	*2*	*2*	*2*	*42*	*19*	this work		*41*				

did alter potentials significantly, oxygen evolution would not be possible since the potential span between P_{680}^{+}/P_{680} and water is only about 0.2 V.

For the second class of models, proton-coupled electron transfer provides the mechanistic basis for each S-state advance (*20*, *46*). Here, small structural changes can have significant effects on kinetics owing to the sensitivity of the proton potential surface to the surrounding heavy-atom distances (*52*−*54*). Thus, although Ca^{2+} is necessary for only the higher S-state transitions (*55*), slight perturbations to its geometry or replacement by Sr^{2+} may affect all S-state transitions. This model places Ca^{2+} in close proximity to the Mn cluster but does not directly use it in O−O bond formation. Its proposed role is to act as a docking site for Cl^{-} so that when Cl^{-} is utilized for charge migration on the S_1 to S_2 transition, its diffusion into the site does not become rate limiting (*20*). The oxygen−oxygen bond is formed, in this model, by the concerted reaction between $Y_z^{\bullet}$, Mn^{IV}═O, and Mn^{IV}-OH (*46*). Siegbahn's (*44*, *56*) concerns about the energetics of Mn^{IV}-$O^{\bullet}$ formation disappear in this model, as an "energetic boost" is provided by the concerted O−O bond formation event. Ca^{2+} is important for efficient O_2 production, but does not play a central role in product formation.

Our results show clearly that all S-state transitions slow when Ca^{2+} is replaced by Sr^{2+}. This result is consistent with those summarized in Table 1, which indicate that all S-state transitions are susceptible to kinetic modification. Moreover, the fact that such a broad range of disparate treatments—biochemical resolution, amino acid replacement, cofactor depletion/repletion, and cofactor replacement—all produce a slowing of the steps preceding O_2 evolution suggests a common mechanism for this effect. The retardation of the S-state-advances occurs without major structural change in the OEC and without a significant perturbation to the energetics of the water-splitting process, as noted above. Coupled with our results (*53*, *57*) and those from several other labs (*58*, *59*) that indicate that $Y_z^{\bullet}$ reprotonates as it is reduced, these observations suggest that a proton coordinate is likely to be involved in these kinetic phenomena. Certainly, similar proton effects have recently been observed (*9*, *60*−*63*) and discussed (*53*) for the oxidation of Y_z by P_{680}^{+}. Accordingly, a more accurate approach to studying the reduction of $Y_z^{\bullet}$ is within the context of proton-coupled, electron transfer (PCET) (*64*).

Three possible mechanistic pathways for PCET reactions are shown in Figure 7. All are possible; which dominates is an issue of competitive rates. Pathways a (ET/PT) and b (PT/ET), along the edges of the diagram, are sequential, and involve either electron first (path a) or proton first (path b) processes. For the sequential pathways, the overall PCET rate constant k can be written as, $k^{-1} = k_{et}^{-1} + k_{pt}^{-1}$, indicating that a slow step will limit the rate. Each of these produces charged intermediates, **2** and **3**, respectively, in the low dielectric of the protein. Our recent considerations (*53*, *65*) have shown that the charge separation required to generate these transition states renders them unlikely in light of the low PSII, S-state-transition activation energies (Table 2). Therefore, these sequential pathways are too slow to be effective channels for the PCET reaction. The remaining pathway, ETPT (path c), involves the concerted transfer of an electron and a proton as a bona fide hydrogen atom. Little charge is accumulated during this process; therefore the activation energies required are expected to be lower, possibly within the values that have been measured for the S-state transitions. We can now explore this pathway in more detail to see if concerted hydrogen-atom transfer provides a rationale for the unusual kinetic parameters that have been obtained for the reduction of $Y_z^{\bullet}$ in PSII.

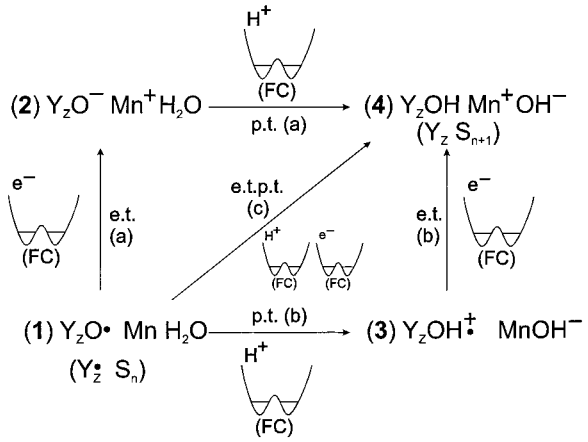

FIGURE 7: Possible reaction paths for electron and proton transfer. Four species are shown as follows: The reactant state $Y_z^{\bullet}$/Mn-(H_2O) **1**, the product state Y_z/$Mn^{+}(OH^{-})$ **4**, and two intermediate states, Y_z^{-}/$Mn^{+}(H_2O)$ **2** and $Y_z^{\bullet+}$/$Mn(OH^{-})$ **3**. Along the edges of the square, two sequential pathways are shown. In path a, electron transfer is followed by proton transfer (ET/PT), while in path b, the reverse sequence of proton and electron steps occurs (PT/ET). In path c, along the diagonal of the square, the electron and proton move in a concerted process (ETPT).

Table 2: Kinetic and Thermodynamic Parameters for the S-State Transitions (taken from refs *2*, *38*, and *53*)

reaction	E_a (kcal M^{-1})	A (s^{-1})	KIE	$Y_z^{\bullet}/Y_z$ (V)	S_{n+1}/S_n (V)
$Y_z^{\bullet}S_0 \rightarrow Y_zS_1$	1.2			0.97	0.70
$Y_z^{\bullet}S_1 \rightarrow Y_zS_2$	3.0	4.0×10^6	1.3; 2.9	0.97	0.93
$Y_z^{\bullet}S_2 \rightarrow Y_zS_3$	9.0	5.4×10^9	1.3	0.97	0.93
$Y_z^{\bullet}S_3 \rightarrow Y_zS_0$			1.4−1.6	0.97	0.93
$T > 280$ K	5.0	8.9×10^5			
$T < 280$ K	9.2	2.9×10^{14}			

The general characteristics of the S-state transitions are summarized in Table 2 and, in many respects, are remarkable. Renger and co-workers have carefully characterized the activation energy E_a and preexponential factor A appearing in the "over the barrier" rate-constant expression $k = A \exp(-E_a/RT)$ for the $S_1 \rightarrow S_2$, $S_2 \rightarrow S_3$, and $S_3 \rightarrow [S_4] \rightarrow S_0$ transitions (*38*). These values are substantially lower than those typically found for an enzyme-catalyzed reaction; textbook values are usually taken to be about 10−12 kcal/mol and 10^{13} M^{-1} s^{-1} for E_a and A, respectively (*66*, *67*). The low A values, in particular, are striking. The low rates for $Y_z^{\bullet}$ reduction and the small kinetic isotope effects that have been measured are also unusual considering the small distance between donor and acceptor (*31*, *68*, *69*) and that proton tunneling has been suggested in $Y_z^{\bullet}$ reduction (*2*). Whether the concerted ETPT mechanism can explain these characteristics now becomes the issue at hand.

Typical kinetic parameters that are observed for H-atom abstraction by radicals are reported in Tables 3 and 4. Considering first the E_a values, the tabulated data span a broad, almost 20 kcal M^{-1}, range. However, for reactions in which a hydrogen atom is abstracted from an oxygen atom

Table 3: Kinetic and Thermodynamic Parameters for H-Atom Abstraction Reactions from an Oxygen Atom by an Oxy-Based Radical

reaction	E_a (kcal M^{-1})	log A (M^{-1} s^{-1})	KIE	k (M^{-1} s^{-1})	ref
4-OMe-phenol + PhO$^\bullet$	nd	nd	nd	4.75×10^5	*82*, *83*
4-H−phenol + PhO$^\bullet$	4.9[a]	nd	nd	3.5×10^5	*82*, *83*
4-*tert*-butyl-phenol + PhO$^\bullet$	4.8	5.5	nd	51.3	*84*
3,5-dimethyl-phenol + PhO$^\bullet$	6.8	6.4	nd	16.3	*83*
α-tocopherol + PhO$^\bullet$	2.0	10.0	1.17	3.1×10^8	*72*
α-naphthol + PhO$^\bullet$	2.2	8.9	nd	2.3×10^7	*72*
ubiquinol-0 + PhO$^\bullet$	3.5	10.5	nd	9.1×10^7	*72*
α-tocopherol + $(C_6H_5)_2CO^\bullet$	nd	nd	1.09	5.1×10^9	*85*
α-tocopherol + $(CH_3)_3CO^\bullet$	nd	nd	1.31	3.8×10^9	*85*
$(CH_3)_3CO$-H + $^\bullet OC(CH_3)_3$	2.6	6.4	nd	nd	*70*

[a] Calculated by the BEBO method.

Table 4: Kinetic and Thermodynamic Parameters for Hydrogen-Atom Abstraction by Radicals

reaction	E_a (kcal M^{-1})	log A (M^{-1} s^{-1})	KIE	k (M^{-1} s^{-1})	ref
CH_3CH_2−H + $^\bullet CH_3$	11.59	11.74	4.04	2.57×10^5	*86*
H_3C−H + $^\bullet CH_3$	14.51	11.80	3.61	7.41×10^3	*86*
SiH_3−H + $^\bullet CH_3$	6.98	11.89	3.10	1.20×10^8	*86*
NH_2−H + $^\bullet CH_3$	9.72	10.76	5.20	2.82×10^5	*86*
SH−H + $^\bullet CH_3$	2.60	11.58	3.65	1.44×10^{10}	*86*
SiH_3−H + $^\bullet CH_2CH_3$	7.24	11.73	1.06	5.89×10^7	*86*
PhS−H + $^\bullet CH_2Ph$	1.5−1.7	9.1−9.4	nd	1.3×10^8	*87*
$(CH_3)_3Sn$−H + $^\bullet CH_3$	3.23	9.39	2.3	1.06×10^7	*88*
$(CH_3)_3Sn$−H + $^\bullet CH_2CH_3$	3.8	9.14	1.9	2.3×10^6	*88*
CH_3CH_2−H + $^\bullet OOCH_3$	14.9	11.46	nd	nd	*89*
CH_3−H + $^\bullet OOCH_3$	18.48	11.26	nd	nd	*89*

by an oxy-based radical, which is the situation we postulate in PSII, the situation simplifies and becomes more homogeneous. The E_a values measured for these types of reactions are most often in the range of 2−7 kcal/mol (Table 3) and are smaller than most of the values shown in Table 4 for other H-atom abstraction reactions, especially those in which a C−H or an N−H bond is the hydrogen-atom donor. This phenomenon has been rationalized by Zavitsas and Chatgilialoglu as being due to triplet repulsion in the transition state (TS) (*70*). As the parallel spins on the donor and acceptor molecules move closer together during formation of the TS, a repulsive energy term becomes more significant to the overall activation energy barrier for the reaction. This term is much smaller for H-atom abstraction between RO$^\bullet$ and −O−H bonds, thereby allowing the oxygen atoms to form a tighter transition state, which lowers the activation energy barrier. On the other hand, as Table 4 shows, H-atom transfer between two carbon atoms, for example, occurs with much higher activation energies. This is due to the stronger triplet repulsion experienced by carbon compared to oxygen. In the case of PSII, reduction of $Y_z^\bullet$ has been proposed to occur via hydrogen-atom abstraction by the tyrosine radical from Mn-ligated water or hydroxide ligands (*20*, *46*). The low activation energies that have been measured in PSII fit well in this context as reflecting what has been measured in other systems in which H-atom transfer between an oxygen-based radical and an −O−H bond occurs. Other theoretical treatments have reached similar conclusions with respect to low E_a values, when hydrogen bonding allows relatively close approach of reactant species in a hydrogen-atom transfer process (*54*, *64*, *71*).

Textbook values for the Arrhenius preexponential factor, A, for hydrogen-atom abstractions are generally low; $A \approx 10^{8.5}$ M^{-1} s^{-1} is often cited as a typical number (*72*). These values are for second-order processes, but with effective PSII concentrations of 1−10 M (*73*), the values reported below for first-order PSII processes become essentially directly comparable to the second-order solution reactions. The fact that the S-state transitions also occur with low A factors provides support for our conclusion that the PSII reactions proceed along the concerted pathway in Figure 7. We can gain physical insight into the meaning of these values for A as follows. The classic interpretation of an A factor is as an "attempt frequency". A low A value implies an unfavorable entropy of activation, which indicates that the system can position itself to enter the transition state only infrequently. For pure electron tunneling at the short $Y_z^\bullet S_n$ distance and for pure proton transfer at short distances, much higher, typically 10^{13} M^{-1} s^{-1}, A values are expected (*48*, *74*), which indicates a much higher attempt frequency. The fact that these larger A values are not found in PSII reinforces our conclusion (*65*) that the sequential pathways, a and b in Figure 7, are not likely in the S-state advances.

Figure 7 rationalizes the A values in terms of the Franck−Condon (FC) factors for proton and electron transfer and follows closely arguments that have been advanced by Cukier (*71*). A rate-constant expression for concerted PCET can be formulated in analogy to the Marcus-Levich pure ET rate constant as (*64*)

$$k_{etpt} = \frac{V_{el}^2}{\hbar}\sqrt{\frac{\pi}{\lambda_s k_B T}}\sum_{n'}\rho_{in'}\sum_{n} \times |\langle\chi_{fn}|\chi_{in'}\rangle|^2 e^{-(\lambda_s+\Delta G^0+\epsilon_{fn}-\epsilon_{in'})^2/4\lambda_s k_B T} \quad (1)$$

The parameters in eq 1 that come from the coupling of the reactant and product charge distributions to the surrounding

medium are the solvent reorganization (λ_s) and reaction-free energies (ΔG^0); V_{el} is the electronic coupling. These are the standard parameters that determine the value of an ET rate constant (*75*, *76*). The new ingredients are Franck−Condon factors of the initial (final) state proton vibronic wave functions χ_{in}' (χ_{fn}). The initial states are summed over the equilibrium initial state proton distribution, ρ_{in}'. The "effective" activation energy appearing in the exponent of eq 1 involves the energetic difference of the proton eigenstates, $\epsilon_{fn} - \epsilon_{in}'$ and arises from the requirement of overall energy conservation between the initial and final electron−proton states. The tunneling of the proton is manifested in the Franck−Condon (FC) factors in eq 1. These factors tend to be small as they are determined by the overlaps of proton wave functions localized around the initial and final proton equilibrium positions, respectively. Thus, concerted PCET is limited by a "Franck−Condon drag" that is a reflection of the requirement that both the electron and the proton are tunneling species. As tunneling is a difficult process, and in concerted PCET there are two tunneling species, the tendency is to obtain relatively small rate constants. However, concerted PCET still can be the dominant reaction channel if the sequential processes are rate limited. As discussed above, both ET/PT and PT/ET sequential processes are indeed rate limited and that leaves the concerted process as the viable channel. Use of reasonable choices for all the parameters in eq 1 does lead to rate-constant values compatible with the magnitudes displayed in Table 2. An important feature of eq 1 is that it does not, strictly speaking, have the form $k = A \exp(-E_a/RT)$. Nevertheless, over typical temperature ranges accessible to biological studies, rate constants based on eq 1 will approximately obey this form. Thus, we may consider that effective activation energies and preexponential factors can be defined for concerted PCET reactions. Evaluation of these factors for appropriate parameter ranges produce values for E_a and A consonant with those in Table 2. In particular, unfavorable entropy of activation factors (low A values) are to be expected for this mechanism. These considerations provide additional support for the notion that the S-state transitions occur by concerted hydrogen-atom transfer (*65*).

The rates and kinetic parameters for overall hydrogen-atom transfers can now be rationalized. If the energetics are not too unfavorable, a sequential pathway is more likely, as the Franck−Condon factors do not hinder the reaction appreciably. This appears to be the case in the bacterial reaction center, where the proton-coupled Q_A^- to Q_B^- reaction follows a sequential route (*77*) and in the Y_Z P_{680}^+ reaction that occurs in PSII (*53*). If, however, the energetics are too unfavorable, as we have argued is the case for the S-state transitions in the OEC, then the concerted pathway is favored. This was also the conclusion drawn by Roth et al. (*78*) and by Sjödin et al. (*79*) for their work on small-molecule model compounds. In these two studies, the authors concluded that the electron transfer/deprotonation process occurred via a concerted mechanism by using similar arguments as those presented above. Thus, for the concerted reaction, the activation energies are generally lower than for the sequential process, but the Franck−Condon drag discussed above lowers the A factors and slows the overall rate considerably. The net result is that rates on the order of 10^3−10^5 s^{-1} are observed for both the S-state advances and for $RO^{\bullet} + R'OH \rightarrow ROH + RO^{\bullet\prime}$ in small organic systems.

In concerted PCET, a substantial isotopic effect can occur, as the deuteron FC factors are smaller than those for a proton. However, these FC factors are strongly dependent on the distance between the flanking heavy atoms that form the hydrogen/deuterium/tritium (H/D/T) bond, with the FC factor increasing for decreasing heavy-atom separation. This increase is more dramatic for T vs D vs H, and studies conducted by Krishtalik on model compounds have shown that the optimum tunneling distance for H, D, and T are different (*52*, *80*). This result leads to the conclusion that it is more favorable for heavier isotopes to spend more energy against the repulsive forces of bringing the flanking atoms together, since tunneling is more difficult than for lighter isotopes. The net result is a decrease in the heavy-atom separation for which tunneling is most effective in the series H, D, T, and this reduces the isotope effect. Furthermore, as the heavy-atom separation decreases, the FC factors saturate to values that are not strongly dependent on distance (*81*). Thus, once the heavy-atom separation is sufficiently small, the distinction between H. D, and T tunnel factors disappears. The rate constants that result from averaging over the heavy-atom separations then lead to kinetic isotope effects that are much more modest than would otherwise be predicted. Thus, small isotope effects for hydrogen-atom abstractions are expected and are confirmed by theoretical calculations with the result of a proton/deuteron rate ratio of no more than a factor of 2, well in agreement with experimental values of 1.7 and 2.3 reported by the Ingold and Mayer groups, respectively (*72*, *78*).

In conclusion, small disturbances of the substrate water/Mn_4 cluster caused, for example, by the substitution of the larger Sr^{2+} ion, produce small changes in the structure of the OEC. These structural perturbations induced by Sr^{2+} substitution or by the other modifications in Table 1 can lead to modification of the activation barrier for hydrogen-atom transfer. Since the donor and acceptor species are intimately coupled in these processes, any change that leads to a higher barrier will slow the rate of hydrogen-atom transfer. This behavior can explain the reduction in rates seen upon depletion of Ca^{2+} or substitution of Sr^{2+} in the OEC, as well as explain the results of the other modifications to the intact system. For PSII, these effects will be seen on all S-state transitions by causing a slowing of the reduction of $Y_z^{\bullet}$ by the substrate water/Mn cluster.

ACKNOWLEDGMENT

We thank Drs. Cecilia Tommos and James Mayer for helpful discussions.

REFERENCES

1. Britt, R. D., Peloquin, J. M., and Campbell, K. A. (2000) *Annu. Rev. Biophsy. Biomol. Struct. 29*, 463.
2. Tommos, C., Hoganson, C. W., Di Valentin, M., Lydakis-Simantiris, N., Dorlet, P., Westphal, K., Chu, H.-A., McCracken, J., and Babcock, G. T. (1998) *Curr. Opin. Chem. Biol. 2*, 244.
3. Yocum, C. F., and Pecoraro, V. L. (1999) *Curr. Opin. Chem. Biol. 3*, 182.
4. Roffey, R. A., Kramer, D. M., Govindjee, and Sayre, R. T. (1994) *Biochim. Biophys. Acta 1185*, 257.

5. Diner, B. A., Nixon, P. J., and Farchaus, J. W. (1991) *Curr. Opin. Struct. Biol. 1*, 546.
6. Chu, H.-A., Nguyen, A. P., and Debus, R. J. (1995) *Biochemistry 34*, 5839.
7. Hays, A. M. A., Vassiliev, I. R., Golbeck, J. H., and Debus, R. J. (1998) *Biochemistry 37*, 11352.
8. Mamedov, F., Sayer, R. T., and Styring, S. (1998) *Biochemistry 37*, 14245.
9. Hays, A.-M., Vassiliev, I. R., Golbeck, J. H., and Debus, R. J. (1999) *Biochemistry 38*, 11851.
10. Homann, P. H. (1987) *J. Bioenerg. Biomembr. 19*, 105.
11. Rutherford, A. W., Zimmermann, J.-L., and Boussac, A. (1992) in *The Photosystems: Structure, Function, and Molecular Biology* (Barber, J., Ed.) pp 179, Elsevier Science Publishers B. V., The Netherlands.
12. Yocum, C. F. (1991) *Biochim. Biophys. Acta 1059*, 1.
13. Nield, J., Orlova, E. V., Morris, E. P., Gowen, B., van Heel, M., and Barber, J. (2000) *Nat. Struct. Biol. 7*, 44.
14. Joliot, P., and Kok, B. (1975) in *Bioenergetics in Photosynthesis*, (Govindjee, Ed.) Academic Press, New York.
15. Kok, B., Forbush, B., and McGloin, M. (1970) *Photochem. Photobiol. 11*, 457.
16. Babcock, G. T., Blankenship, R. E., and Sauer, K. (1976) *FEBS Lett. 61*, 286.
17. Razeghifard, M. R., Klughammer, C., and Pace, R. J. (1997) *Biochemistry 36*, 86.
18. Razeghifard, M. R., and Pace, R. J. (1997) *Biochim. Biophys. Acta 1322*, 141.
19. Razeghifard, M. R., Wydrzynski, T., Pace, R. J., and Burnap, R. L. (1997) *Biochemistry 36*, 14474.
20. Tommos, C., and Babcock, G. T. (1998) *Accounts Chem. Res. 31*, 18.
21. Qian, M., Dao, L. A., Debus, R. J., and Burnap, R. L. (1999) *Biochemistry 38*, 6070.
22. Ghanotakis, D. F., Babcock, G. T., and Yocum, C. F. (1984) *FEBS Lett. 167*, 127.
23. Boussac, A., and Rutherford, A. W. (1988) *Biochemistry 27*, 3476.
24. Boussac, A., Sétif, P., and Rutherford, A. W. (1992) *Biochemistry 31*, 1224.
25. Berthold, D. A., Babcock, G. T., and Yocum, C. F. (1981) *FEBS Lett. 134*, 231.
26. Ghanotakis, D. F., Topper, J., Babcock, G. T., and Yocum, C. F. (1984) *Biochim. Biophys. Acta 767*, 524.
27. Hoganson, C. W., and Babcock, G. T. (1988) *Biochemistry 27*, 5848.
28. Babcock, G. T. (1987) in *New Comprehensive Biochemistry* (Amesz, J., Ed.) pp 125, Elsevier, Amsterdam.
29. Warden, J. T., Blankenship, R. E., and Sauer, K. (1976) *Biochim. Biophys. Acta 423*, 462.
30. Gilchrist, M. L., Jr., Ball, J. A., Randall, D. W., and Britt, R. D. (1995) *Proc. Natl. Acad. Sci. U.S.A. 92*, 9545.
31. Dorlet, P., Di Valentin, M., Babcock, G. T., and McCracken, J. L. (1998) *J. Phys. Chem. B 102*, 8239.
32. Lakshmi, K. V., Eaton, S. S., Eaton, G. R., and Brudvig, G. W. (1999) *Biochemistry 38*, 12758.
33. Rappaport, F., Blanchard-Desce, M., and Lavergne, J. (1994) *Biochim. Biophys. Acta 1184*, 178.
34. Hillier, W., Messinger, J., and Wydrzynski, T. (1998) *Biochemistry 37*, 16908.
35. Tommos, C., McCracken, J., Styring, S., and Babcock, G. T. (1998) *J. Am. Chem. Soc. 120*, 10441.
36. Hillier, W., and Wydrzynski, T. (2000) *Biochemistry 39*, 4399.
37. Haumann, M., Bogershausen, O., Cherepanov, D., Ahlbrink, R., and Junge, W. (1997) *Photosynth. Res. 51*, 193.
38. Karge, M., Irrgang, K. D., and Renger, G. (1997) *Biochemistry 36*, 8904.
39. Lydakis-Simantiris, N., Ghanotakis, D. F., and Babcock, G. T. (1997) *Biochim. Biophys. Acta 1322*, 129.
40. Dekker, J. P., Ghanotakis, D. G., Plijter, J. J., Van Gorkom, H. J., and Babcock, G. T. (1984) *Biochim. Biophys. Acta 767*, 515.
41. Wincencjusz, H., Yocum, C. F., and van Gorkom, H. J. (1999) *Biochemistry 38*, 3719.
42. Hundelt, M., Hays, A.-M., Debus, R. J., and Junge, W. (1998) *Biochemistry 37*, 14450.
43. Pecoraro, V. L., Baldwin, M. J., Caudle, M. T., Hsieh, W.-Y., and Law, N. A. (1998) *Pure Appl. Chem. 70*, 925.
44. Siegbahn, P. E. M., and Crabtree, R. H. (1999) *J. Am. Chem. Soc. 121*, 117.
45. Limburg, J., Vrettos, J. S., Liable-Sands, L. M., Rheingold, A. L., Crabtree, R. H., and Brudvig, G. W. (1999) *Science 283*, 1524.
46. Hoganson, C. W., and Babcock, G. T. (1997) *Science 277*, 1953.
47. Limburg, J., Szalai, V. A., and Brudvig, G. W. (1999) *J. Chem. Soc., Dalton Trans. 9*, 1353.
48. Page, C. C., Moser, C. C., Chen, X., and Dutton, P. L. (1999) *Nature 402*, 47.
49. Latimer, M. J., Derose, V. J., Mukerji, I., Yachandra, V. K., Sauer, K., and Klein, M. P. (1995) *Biochemistry 34*, 10898.
50. Riggs-Gelasco, P. J., Mei, R., Ghanotakis, D. F., Yocum, C. F., and Penner-Hahn, J. E. (1996) *J. Am. Chem. Soc. 118*, 2400.
51. Cinco, R. M., Robblee, J. H., Rompel, A., Fernandez, C., Yachandra, V. K., Sauer, K., and Klein, M. P. (1998) *J. Phys. Chem. 102*, 8248.
52. Krishtalik, L. I. (2000) *Biochimica. Biophysica. Acta 1458*, 6.
53. Tommos, C., and Babcock, G. T. (2000) *Biochim. Biophys. Acta 1458*, 199.
54. Scheiner, S. (2000) *Biochimica. Biophysica. Acta 1458*, 28.
55. Boussac, A., Zimmermann, J.-L., Rutherford, A. W., and Lavergne, J. (1990) *Nature 347*, 303.
56. Siegbahn, P. E. M. (2000) *Inorg. Chem. 39*, 2923.
57. Barry, B. A., and Babcock, G. T. (1987) *Proc. Nat. Acad. Sci. U.S.A. 84*, 7099.
58. Un, S., Tang, X.-S., and Diner, B. A. (1996) *Biochemistry 35*, 679.
59. Berthomieu, C., Hienerwadel, R., Boussac, A., Breton, J., and Diner, B. A. (1998) *Biochemistry 37*, 10547.
60. Rappaport, F., and Lavergne, J. (1997) *Biochemistry 36*, 15294.
61. Schilstra, M. J., Rappaport, F., Nugent, J. H. A., Barnett, C. J., and Klug, D. R. (1998) *Biochemistry 37*, 3974.
62. Christen, G., and Renger, G. (1999) *Biochemistry 38*, 2068.
63. Christen, G., Seeliger, A., and Renger, G. (1999) *Biochemistry 38*, 6082.
64. Cukier, R. I., and Nocera, D. G. (1998) *Annu. Rev. Phys. Chem. 49*, 337.
65. Westphal, K. L., Tommos, C., Cukier, R. I., and Babcock, G. T. (2000) *Curr. Opin. Plant Biology 3*, 236.
66. Segel, I. H. (1975) *Enzyme Kinetics, Behavior and Analysis of Rapid Equilibrium and Steady-State Enzyme Systems*, John Wiley & Sons, New York.
67. Chance, B., DeVault, D. C., Frauenfelder, H., Marcus, R. A., Schrieffer, J. R., and Sutin, N. (1979) *Tunneling in Biological Systems*, Academic Press, New York.
68. Peloquin, J. M., Campbell, K. A., and Britt, R. D. (1998) *J. Am. Chem. Soc. 120*, 6840.
69. Lakshmi, K. V., Eaton, S. S., Eaton, G. R., Frank, H. A., and Brudvig, G. W. (1998) *J. Phys. Chem. B 102*, 8327.
70. Zavitsas, A. A., and Chatgilialoglu, C. (1995) *J. Am. Chem. Soc. 117*, 10645.
71. Cukier, R. I. (1999) *J. Phys. Chem. A 103*, 5989.
72. Foti, M., Ingold, K. U., and Lusztyk, J. (1994) *J. Am. Chem. Soc. 116*, 9440.
73. Rüttinger, W., and Dismukes, G. C. (1997) *Chem. Rev. 97*, 1.
74. Silverman, D. N. (2000) *Biochim. Biophys. Acta 1458*, 88.
75. Ulstrup, J. (1979) *Charge-Transfer Processes in Condensed Media*, Springer, Berlin.
76. Marcus, R. A., and Sutin, N. (1985) *Biochim. Biophys. Acta 811*, 265.
77. Okamura, M. Y., Paddock, M. L., Graige, M. S., and Feher, G. (2000) *Biochim. Biophys. Acta 1458*, 148.
78. Roth, J. P., Lovell, S., and Mayer, J. M. (2000) *J. Am. Chem. Soc. 122*, 5486.
79. Sjödin, M., Styring, S., Åkermark, B., Sun, L., and Hammarström, L. (2000) *J. Am. Chem. Soc. 122*, 3932.

80. Krishtalik, L. I. (1979) *J. Electroanalyt. Chem. 100*, 547.
81. Cukier, R. I., and Zhu, J. (1997) *J. Phys. Chem. 101*, 7180.
82. Mahoney, L. R., and DaRooge, M. A. (1975) *J. Am. Chem. Soc. 97*, 4722.
83. Mahoney, L. R., and DaRooge, M. A. (1972) *J. Am. Chem. Soc. 94*, 7002.
84. Mahoney, L. R., and DaRooge, M. A. (1969) *J. Am. Chem. Soc. 92*, 890.
85. Evans, C., Scaiano, J. C., and Ingold, K. U. (1992) *J. Am. Chem. Soc. 114*, 4589.
86. Arthur, N. L., and Bell, T. N. (1978) *Rev. Chem. Intermed. 2*, 37.
87. Franz, J. A., Bushaw, B. A., and Alnajjar, M. S. (1989) *J. Am. Chem. Soc. 111*, 268.
88. Chatgilialoglu, C., Ingold, K. U., and Scaiano, J. C. (1981) *J. Am. Chem. Soc. 103*, 7739.
89. Mims, C. A., Mauti, R., Dean, A. M., and Rose, K. D. (1994) *J. Phys. Chem. 98*, 13357.

BI0018077